**Anne GAYMARD**

SML/POC Master student, 1st year
2nd semester 2022

**Institut Universitaire Européen de la Mer**
Technopôle Brest-Iroise,
Rue Dumont D'urville - 29280 Plouzané

M1 Internship Report
May - June 2022

---

# **Title:** Dispersion of floating (plastic) particles on the surface of the ocean under the influence of currents and waves

---

**Laboratoire d'Océanographie Physique et Spatiale**
Technopôle Brest-Iroise

## Supervisors

| | |
|---|---|
| Thierry HUCK | CR CNRS-LOPS |
| Florian SÉVELLEC | CR CNRS-LOPS |

# Acknowledgement

First and foremost, I would like to thank my supervisors. They followed my work throughout my internship at the Laboratory, advised and guided me throughout my internship. Many thanks to Dr T. HUCK, who made it possible for me to gain research experience in the plastic domain. His explanations of the modelling notion behind my mission helped me understand it better. Many thanks to Dr F. SEVELLEC, to follow my work as well and for his theoretical explanations. Working with them has been a real pleasure, making me want to continue in the field of plastics

Many thanks also to all the PhD students and researchers in the LOPS. They were sources of ideas during the Tuesday presentations, allowing a broader view of my work.

Lastly, I would like to thank all the students in my office, Bastien, Benoit, Maud, Max and Quentin. They made it possible for me to work in good conditions during my internship and helped me with coding and theory parts. I would also like to thank the other students in internship for creating a good group dynamic.

**Abstract**

As production continues to increase, more and more plastics are finding their way into the ocean gyres. This work tries to understand the impact of the waves and the current on these floating particles in the Atlantic, in particular their impact in terms of dispersion. To measure this impact, a lagrangian approach is performed using two numerical experiments with ARIANE, the LOPS Lagrangian particle software. For both experiments, floating particles are spread over the entire surface of the Atlantic Ocean and followed for 20 days and 3 months. The first one uses only the ocean current for the particles advection, whereas the second one adds the net transport by the waves, the Stokes drift. These experiments used data from the NEMO platform for the ocean currents and Météo France data for the Stokes drift. The results of dispersion are compared with the eddy kinetic energy (EKE) and the strain magnitude of the flow. We find that the impact of the Stokes drift is negligible compared to the impact of the ocean currents for the dispersion. Consistently the EKE shows a factor of 10 between the energy of the currents and those induced by the Stokes drift. This same scaling factor is also observed for the strain magnitude. Our results on dispersion have to be put in the context of the "mean" flow, for which Dobler et al. (2019) show that Stokes drift changes the direction of the "mean" particle flow. This work can be extended to different locations to get a global vision of the dispersion.

**Keywords**: Dispersion, Plastics, Stokes Drift, North Atlantic ocean, Lagrangian displacement.

# Contents

# 1. Introduction

Plastics are ubiquitous today. Even in the most remote areas, it is still possible to see the human impacts. Pollution continues to increase as long as plastic production continues to grow. In 2018, 360 million plastics tonnes have been produced, with 5 to 12 tonnes of Mismanaged Plastic Waste released into the ocean by the wind and the polluted rivers. Our pollution conquers marine life and is subject to processes of physical, chemical and biological decomposition. These processes are still difficult to understand and parameterise.

Some works have been carried out about the plastic displacement in the Indian Ocean, such as in the paper of Dobler et al. (2019). This area is very studied regarding plastic pollution because most of the plastic inflow has been located in its surrounding estuaries. A large part of this waste is going to the Pacific ocean, creating the "plastic continent" but also in the Indian ocean. However, Indonesia is not responsible for all the pollution, all countries and continents pollute and plastic continents are present in each ocean. They are located in the large converging subtropical gyres.

There are two methods to describe particle displacements, the Lagrangian method and the Eulerian method. The Eulerian method is based on particle concentration evolving at fixed locations. The concentration evolution is recorded during its evolution. The Lagrangian method is based on following individual particles. The particle trajectory (i.e. position) is recorded throughout the time evolution. As floating debris, plastic particles are subject to surface current but also the waves, through its nonlinear effect called Stokes drift, indirectly caused by the wind. In Dobler et al. (2019), two experiments have been carried out using ARIANE software, which is based on Lagrangian particle approach. In the first one, the displacement of particles has been studied with the ocean current only; whereas in the second one, the Stokes drift was included. They show that the Stokes drift shifts the particles westward whereas, the current only shifts particles eastward, see Fig. 1.

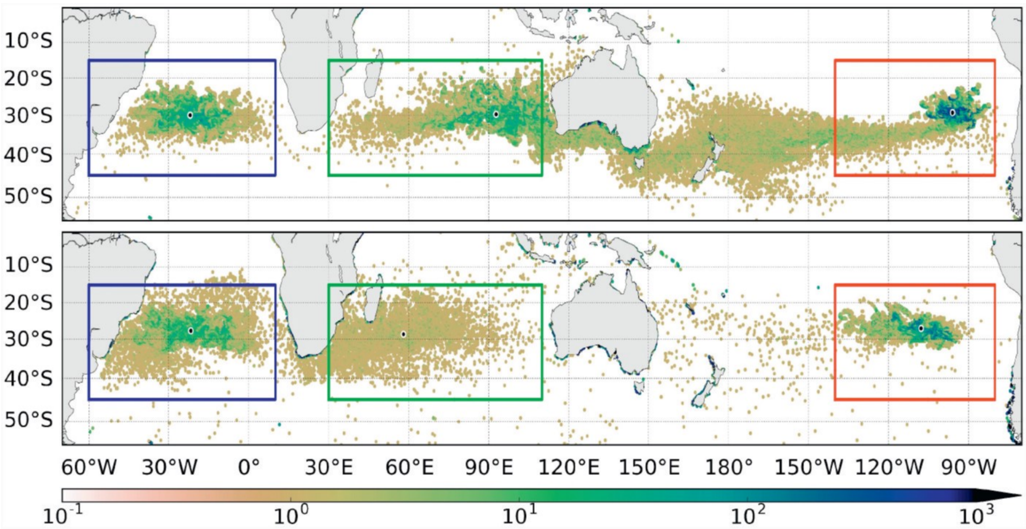


Figure 1: The concentration of particles for the simulation of the ocean current only (top) and the simulation including the Stokes drift (bottom). The color corresponds to the particle number. The black dots correspond to the center of mass. These simulations have been carried out during 29 years, running 5 times between 2010 and 2016. Reproduced after Dobler et al. (2019).

Unlike previous work, that mainly focus on debris "mean" displacements, the main goal of our work is to characterize and understand the dispersion impact of the Stokes's drift in the ocean. In this research work, we focus on the North Atlantic ocean. Indeed, the Atlantic ocean is an interesting case study because it includes three important parameters for our study: there is mesoscale turbulence, there is Stokes drift, and there is plastic pollution. Here, Lagrangian debris displacement will be modelled through numerical simulations.

# 2. Method

## 2.1. The ARIANE Lagrangian Modelling software

To follow the evolution of "plastic" particles in the North Atlantic, ARIANE software has been used. The model uses a Lagrangian method to solve particle displacements. The particle velocities are described as (Blanke and Grima, 2005):

$$U_p = \frac{\partial x}{\partial t} \quad (1)$$

$$V_p = \frac{\partial y}{\partial t} \quad (2)$$

$$W_p = \frac{\partial z}{\partial t} \quad (3)$$

$$(4)$$

where $t$ is time, $x$, $y$ and $z$ zonal, meridional and vertical position of a particle at any time and $U_p$, $V_p$, and $W_p$ are there associated Lagrangian velocities.

ARIANE software is designed for using velocities from C-grid (Arakawa, 1972) ocean models, as described in the fig. 2. This grid is often used in ocean models (NEMO, CROCO) and allows the conservation of mass, freshwater, and heat. Moreover, the boundary conditions induced null-velocity along the coasts. The zonal velocity, $u$, is located from the west to the east borders of the meshes (from left to right in Fig. 2, respectively) and the meridional velocity, $v$, is located from the south to the north borders (from bottom to top in Fig. 2, respectively). In Ariane, inside the cell, the velocities are interpolated linearly from one edge to the other. More generally, in a C-grid context, the temperature, salinity, density and pressure data are located at the center of the grid, whereas the vorticity is recorded at the corner of the grid. The cells are not uniform in longitudes and latitudes, and so are not uniform in area since the Earth is a sphere. Adding to the zonal and meridional dimensions, the grid also has a non-uniform vertical coordinate, with grid thickness varying with depth. Surface currents are located in the first meter of depth.

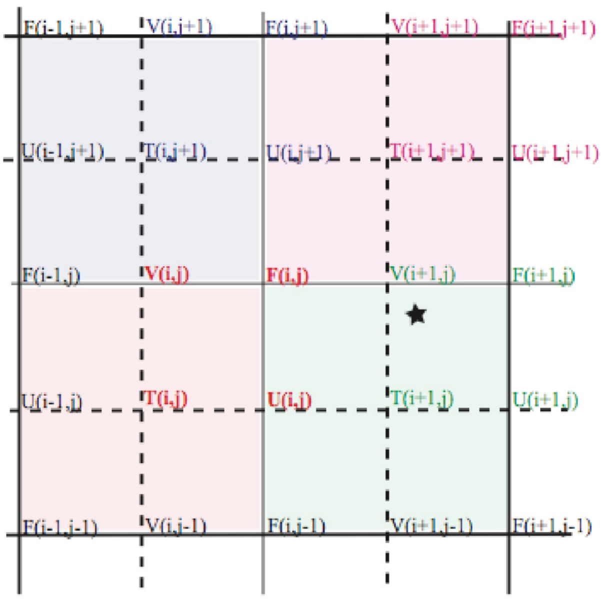


Figure 2: The C grid used by ARIANE, from Blanke and Grima (2005)

## 2.2. The Lagrangian experiments set up

The whole North Atlantic ocean has been covered by virtual/simulated plastic particles. To represent the floating "plastic" particles, the depth has been fixed to 1 meter. Hence, particles can only evolve along the zonal and the meridional directions.

During this internship, two different experiments have been set.

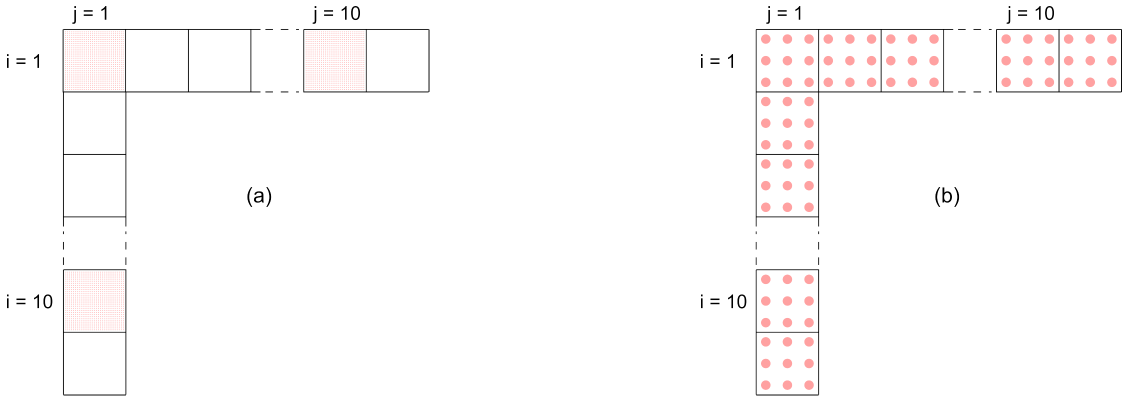


Figure 3: Initial particle positions on the mesh grid for the two experiments: (a) experiment 1, with 31×31 particles in the mesh every 10 gridcells in each direction; (b) experiment 2, with 3×3 particles in every gridcell.

In the first experiment, groups of 31×31 plastic particles have been distributed at each longitude and latitude of the North Atlantic ocean. All the particle ensembles are located inside a single gridcell and separated every 10 gridcells, as represented in the Fig. 3a. Each group (corresponding to 961 particles) will evolve, dispersing more or less according to the underlying flow of their geographical location. This experiment is carried out for one year and the trajectories are recorded every two days.

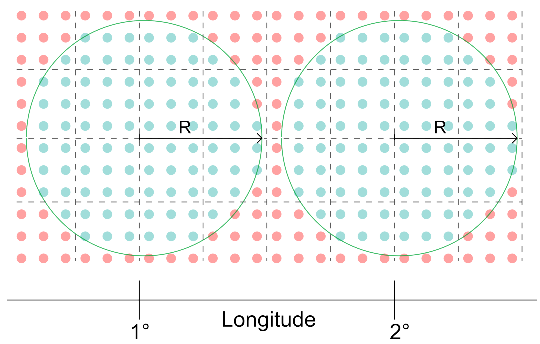


Figure 4: The distribution of the group particle selection for the experience 1. The radius, $R$, is 50 km.

Analyzing the first results from this experiment, we realised that the groups of particles were evolving following two regimes. First, the particles moved together with almost no dispersion, before dispersion occurred. As explained before, inside a cell the velocities are interpolated. Thus, the displacement inside a cell is not physical but only based on the interpolation reconstruction. In this context we were not sure if the regime with the lack of dispersion was not purely due to the interpolation techniques with no relation to a physical behaviour. To avoid taking the interpolation method as a physical characteristic, another experiment was set, allowing for a broader group of particle (more consistent with the resolved-scale of the velocities).

Hence, for the second experiment, only 3×3 particles are located inside each cell. All the cells are filled, as shown in the Fig. 3b. The experiment is carried out during six months, with daily data outputs. To visualise the dispersion, sub-groups were delimited counting around 1,000 particles. In the first experience, the sub-groups were delimited directly by using the cell, but for the second experience, the separation is made using a circle with a radius of 50 km. Circles are centered along a 1°×1° horizontal grid, as represented in the Fig. 4. As the grid area is not uniform, the number of particles in the groups changes accordingly to their latitude.

This configuration is designed to avoid (as much as possible) the reconstruction errors possibly observed in the previous experiment. Only the second experiment is used and described in the following.

To represent buoyant particles, they are located at the ocean surface. In general, they are affected not only by sea currents, but also by the forces created by the wind. The windage is the displacement generated by the wind on the emerged parts of the debris. For this study, we assume that the particles are submerged near the surface and are not subject to this direct force of the wind. However, the wind energy can be transferred to the sea by creating waves (and Ekman motion). During the passage of the waves, in a linear framework, the water particles should remain in place, as the wave does not cause any material transfer. However, in reality, close to the surface, a slight shift is observed. This nonlinear drift is the Stokes drift. Thus, the dispersion of the particles in the North Atlantic ocean is studied in a first experiment taking only into account the ocean current, and in a second experiment where the Stokes drift is added simply to the ocean current.

## 2.3. The velocity fields used

The zonal velocity $U_p$ and the meridional velocity $V_p$ come from two different models. The data of the ocean current come from the Global Ocean General Circulation Model Reanalysis, at 1/12°, MERCATOR-GLORYS12V1 from the Copernicus Program. This model is based on the NEMO platform forced at its surface by the ERA-Interim atmospheric reanalysis of the European Center for Medium-range Weather Forecast (Chenillat et al., 2021). This reanalysis covers almost 30 years from 1993 to 2022 with daily-frequency velocity outputs. In this work, the time span of the experiments is six months from 1 January 1993.

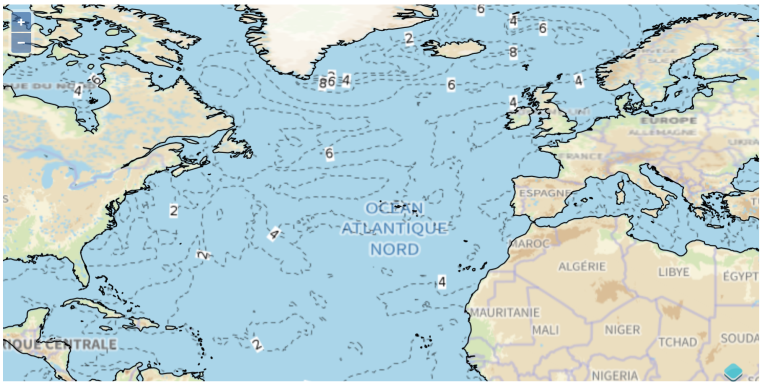


Figure 5: Example of data set of the wave velocity magnitude (in m/s) from MFWAM

In the second experiment, we have added the surface Stokes drift to the ocean velocity. These data are recovered from the Global Ocean Waves Reanalysis, WAVERYS, also from Copernicus Program. This model is based on Météo France WAM wave model, as shown in Fig. 5. As the weather changes very fast, the wind-forced wave speeds are recorded every 3 hours. These are averaged every 24 hours to fit with the daily ocean velocity data. Moreover, the resolution of the wave model is 1/5°, so to not deteriorate the 1/12° ocean-velocity data, the Stokes drift has been linearly interpolated from its native grid onto the 1/12° ocean grid.

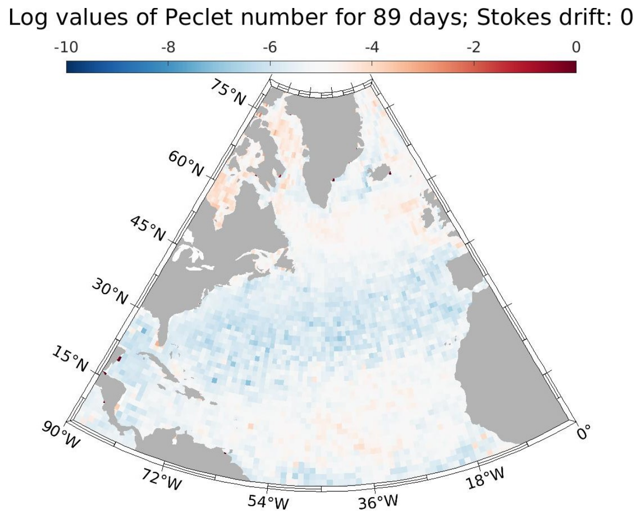


(a) Ocean current

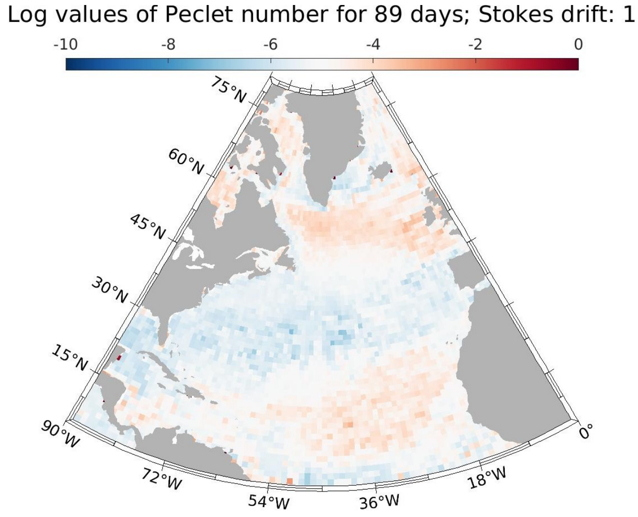


(b) Adding Stokes drift

Figure 6: The Péclet number for (a) the experiment with solely the ocean currents and (b) the experiment where the Stokes drift is added to the ocean currents. The scale of the graph is in log10.

## 2.4. The diffusivity estimation

The diffusion equation which drives the tracer concentration has been used in several paper as Lacasce (2008) and Sévellec et al. (2022) and is defined as :

$$\partial_t C = \nabla \cdot \mathbf{K} \cdot \nabla C, \tag{5}$$

where $C$ is the tracer concentration and $\mathbf{K}$ is a horizontal diffusivity tensor. This tensor is difficult to estimate and can be decomposed into a zonal, meridional, and cross components or can be simply approximated to a single value.

The estimated diffusivity in the ocean can be calculated using at least two single-particle trajectory. Here, the particle ensembles, defined in fig. 4, are considered as representative of a concentration and the diffusion is estimated by the rate of dispersion from its center of mass (Roach et al., 2018):

$$K(t) = \frac{1}{2}\frac{d\langle X(t)^2\rangle}{dt}, \tag{6}$$

where $K$ is the diffusivity and $X$ is the particle distance relative to the mass centre. This distance is calculated for each day. The depth being fixed, only the zonal and meridional directions are studied for the diffusion of the particles. Then, the linear trend of the distance variance is used to estimate the diffusivity, $K$.

However, our Lagrangian framework does not strictly allow the use of (5) because it does not consider the advection. Then, by considering the advection, the equation becomes $D_t C = \nabla \cdot \mathbf{K} \cdot \nabla C$ where $D_t$ is the material derivation and $\mathbf{K}$ is the diffusivity (Sévellec et al., 2022). Hence, in this study, the diffusivity is defined as $K'$ and calculated along a moving mass centre, as described in (6). Ideally, the $K$ and $K'$ values should be close so that we remain in the classical framework of (5). In other words, ideally the mean advection could be neglected over the dispersion. To test that we can compute the Péclet number, which is defined as the ratio between the advective and diffusive transport rates (Fig. 6). This shows that the Stokes drift provides more advection transport than the diffusivity compared to an ocean current. The global results observed on these two maps show that diffusivity predominates over advection, with a Peclet number $\ll 1$. Thus, $K$ and $K'$ values are close allowing one to consider a local study.

The qualitative way of estimating diffusion is to refer to the eddy kinetic energy (EKE). Indeed the EKE measures the amount of velocity variations the particle ensemble feels at a given location. Hence, and as described in Zhurbas et al. (2014), EKE is a way to estimate the diffusivity. EKE reads:

$$\mathrm{EKE} = \frac{1}{2}\left(\overline{u'}^2 + \overline{v'}^2\right) \tag{7}$$

where $u'$ and $v'$ are the zonal and meridional anomalous velocities, respectively. The anomaly is defined as the difference from the time-mean at each location. This energy is associated with turbulent flow.

Alternatively, a quantitative way to estimate the particle ensemble deformation is through the strain. The link between the tracer concentration and the strain has been studied in a range of papers by using the tracer advection equation: Okubo (1970), Weiss (1991) and Balwada et al. (2021), for instance. Here we summarized their results (following the notes from Florian Sévellec in Appendix A):

$$\partial_t C + \partial_x(uC) + \partial_y(vC) + \partial_z(wC) = 0 \tag{8}$$

where $t$ is the time; $x$, $y$, and $z$ are the longitude, latitude, and depth, respectively; and $u$, $v$, and $w$ are the zonal, meridional, and vertical Eulerian velocities, respectively. The fluid is considered to be an incompressible fluid where $\partial_x u + \partial_y v + \partial_z w = 0$. Moreover, the plastic particles are floating, allowing to neglect of the variation along the $z$-axis. Then, the tracer gradient equation can be written as:

$$D_t \begin{pmatrix} \partial_x C \\ \partial_y C \end{pmatrix} = \boldsymbol{\Lambda} \begin{pmatrix} \partial_x C \\ \partial_y C \end{pmatrix}, \tag{9}$$

where $\boldsymbol{\Lambda}$ is the flow gradient operator. The parameter of $\boldsymbol{\Lambda}$ can be defined by the properties of the flow:

$$\boldsymbol{\Lambda} = -\frac{1}{2}\begin{pmatrix} \Delta + \sigma_n & \sigma_s + \zeta \\ \sigma_s - \zeta & \Delta - \sigma_n \end{pmatrix} \tag{10}$$

where $\Delta$ is the divergence, $\zeta$ is the vorticity, $\sigma_n$ is the normal strain (stretching), and $\sigma_s$ is the shearing strain. The strain magnitude can be, then, defined with $\sigma_n$ and $\sigma_s$ as $\sigma = \sqrt{\sigma_n^2 + \sigma_s^2}$.

The matrix $\boldsymbol{\Lambda}$ can be decomposed as the sum of symmetric and skew-symmetric matrices. The skew-symmetric matrix defines the rotation of the gradient concentration of the particle ensemble while the symmetric matrix defined the deformation of the gradient concentration of the particle ensemble by the dilatation, shearing, and stretching. This latter operator is defined as:

$$\boldsymbol{\Sigma} = \frac{\boldsymbol{\Lambda} + \boldsymbol{\Lambda}^\dagger}{2} = -\frac{1}{2}\begin{pmatrix} \Delta + \sigma_n & \sigma_s \\ \sigma_s & \Delta - \sigma_n \end{pmatrix} \tag{11}$$

Moreover, $\boldsymbol{\Sigma}$ can be diagonalised, providing two eigenvectors and their associated orthogonal directions (because $\boldsymbol{\Sigma}$ is symmetric). The eigenvalues give the rate of the deformation and the eigenvectors give the direction of these deformations. These former values are defined with $\Delta$ and $\sigma$. But, since $|\Delta| \ll \sigma$, the deformation is mainly controlled by the strain magnitude (See notes from Florian Sévellec for a more detailled derivation, Appendix A).

This last relation suggests that the strain variations lead to the stretching and shearing of the particle ensemble, increasing the distance of the particles from their barycentre. Thus, these variations of the gradient magnitude lead to the spreading of the concentration.

# 3. Results

## 3.1. Particles dispersion and diffusivity

The dispersion is illustrated in three locations where the currents are very different: in the Gulf Stream, in the middle-north of the subtropical gyre, and in the south-middle of the subtropical gyre (Fig.7a). The dispersion of the particles is represented for both experiments, the one with solely the ocean currents and the one where the Stokes drift is added to the ocean currents.

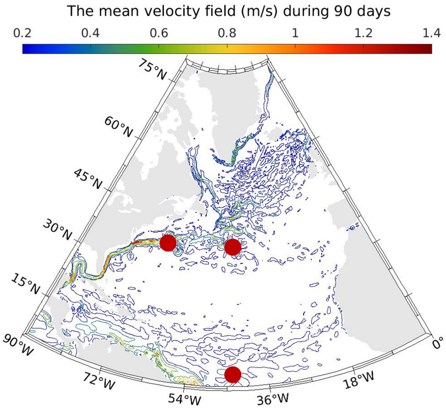


(a) Location for the dispersion analysis.

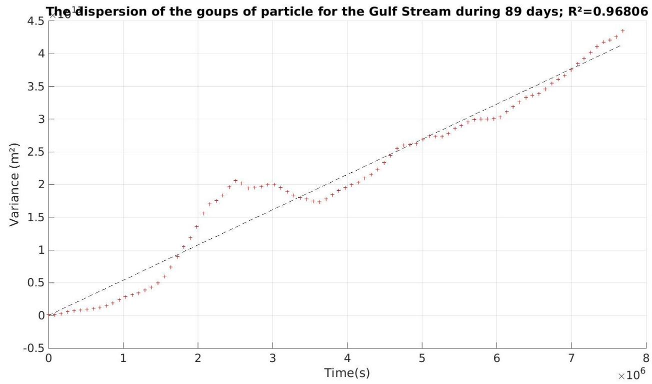


(b) The horizontal diffusivity, **K**, is estimated with the linear slope.

Figure 7: Description of the diffusivity measures.

In Fig. 8 and Fig. 9, the dispersion seems larger for the expriment with Stokes drift. The result obtained for Fig. 8 is consistent with the currents observed in this area: the particles distinctly draw the meanders of the Gulf Stream. Figure 10 has a different behaviour with a larger dispersion for the result without Stokes drift. Moreover, there is very little dispersion in the first few days in both experiments, the group of particles moves in a single block before dispersing, suggesting two distinct regimes.

From these first observations, the diffusivity is calculated as explained in the part below for each group of particles, as shown in Fig.7b. Fig. 11 shows a global diffusivity on the Atlantic ocean, where each point corresponds to the diffusivity along the path of the particle ensemble but represented at its initial location. This computation is done over 19 days or 90 days and for both experiments. This shows that the observed dispersion have the same trend with and without Stokes drift. The main dispersion areas are located in the Gulf Stream and in the southern subtropical gyre. However, the difference in amplitude is significant for the 3-month computation. The long integration time expels the particles more or less far depending on their location, and the idea of representing them at their initial location is questionable. To quantify the "locality" of our computation we used the Péclet number, which is explained below.

To validate the results obtained, the residual coefficient is calculated for the evolution of each group of particles. This coefficient, $R^2$, is the difference between the data and the associated linear regression, defined as:

$$R^2 = 1 - \frac{SS_{resid}}{SS_{total}} \tag{12}$$

where $SS_{resid}$ is the sum of the squared residuals and $SS_{total}$ is the sum of the squared differences from the mean of the dependent variable. The values of the coefficient are between 0 and 1, where 1 is a good approximation with small errors. As shown in Fig. 11, the majority of the map is covered by values close to 1.

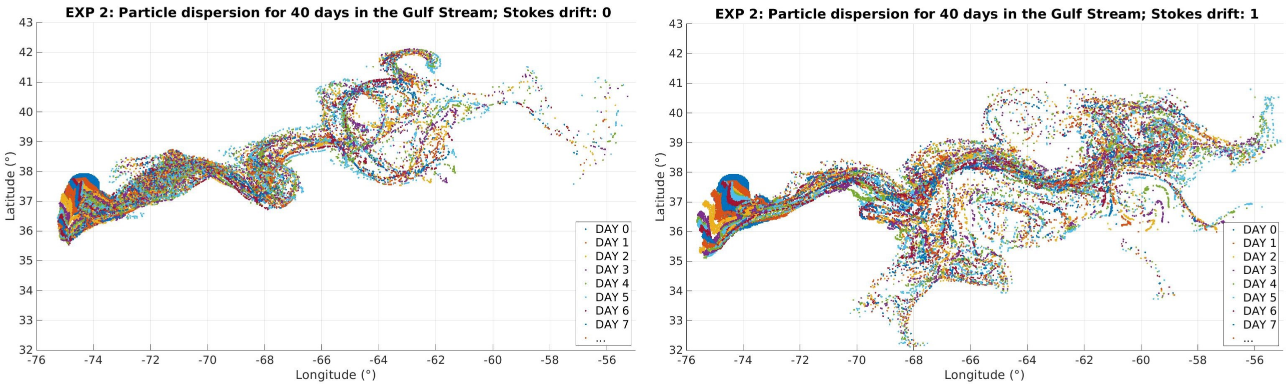


(a) Ocean current

(b) Adding Stokes drift

Figure 8: The dispersion in the Gulf Stream for (a) the experiment with solely the ocean currents and (b) the experiment where the Stokes drift is added to the ocean currents. Each colour represents the dispersion at a given day.

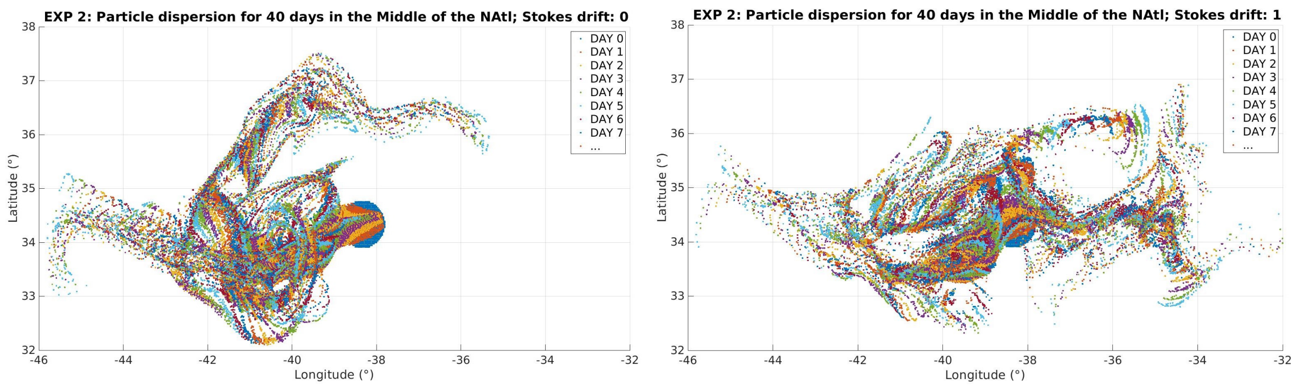


(a) Ocean current

(b) Adding Stokes drift

Figure 9: The dispersion in the north subtropical gyre for (a) the experiment with solely the ocean currents and (b) the experiment where the Stokes drift is added to the ocean currents. Each colour represents the dispersion at a given day.

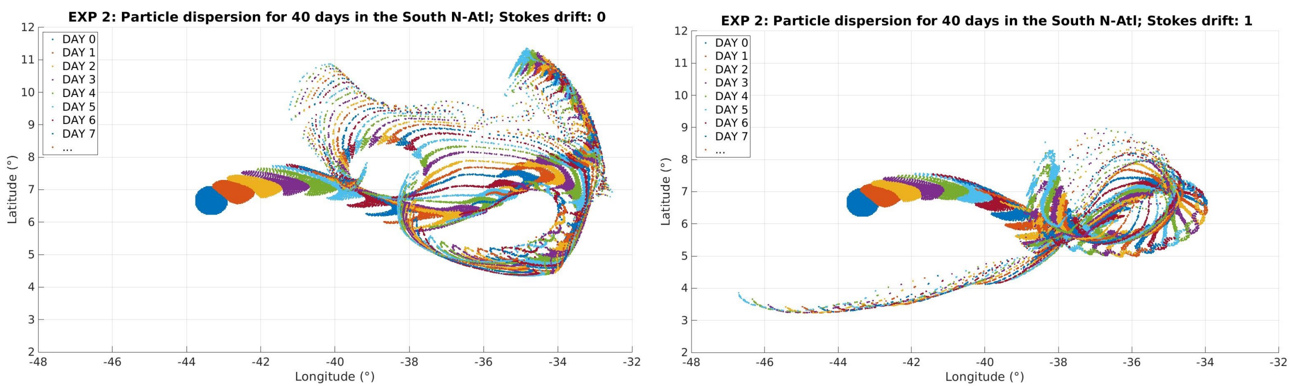


(a) Ocean current

(b) Adding Stokes drift

Figure 10: The dispersion in the south subtropical gyre for (a) the experiment with solely the ocean currents and (b) the experiment where the Stokes drift is added to the ocean currents. Each colour represents the dispersion at a given day.

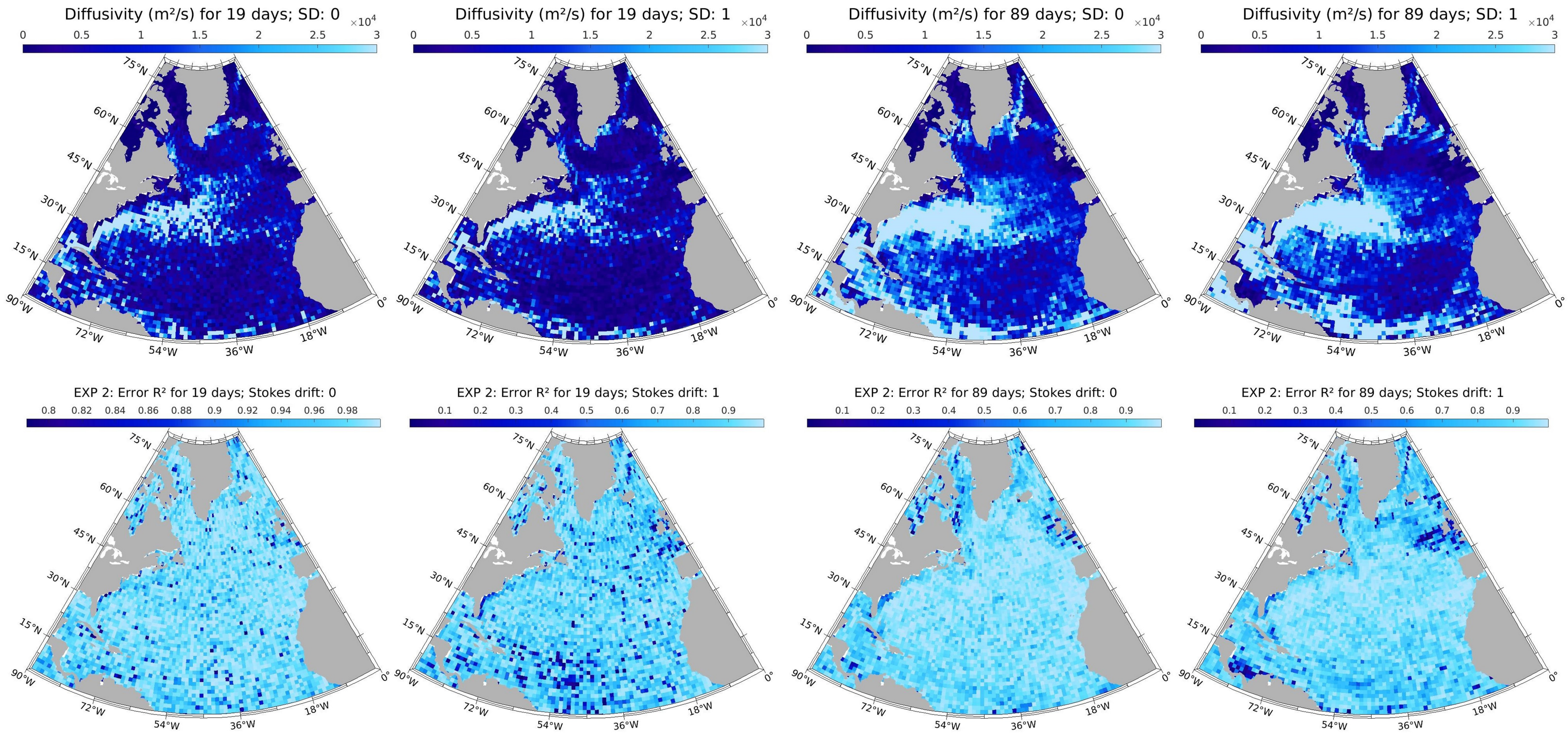


Figure 11: (top row) the diffusion of the particles (measured as the trend of the particle ensemble distance variance) after 19 days for the two experiments (with and without Stoke drift) and after 90 days. (bottom row) the associated error comparing the linear trend with the variance evolution of the particle ensemble distance, computed with the coefficient of determination ($R^2$) which measured the proportion of explained variance. For each figure, the model of the ocean current is defined by *Stokes Drift:0* or *SD:0* and the one adding the Stokes drift is defined as *Stokes Drift:1* or *SD:1*.

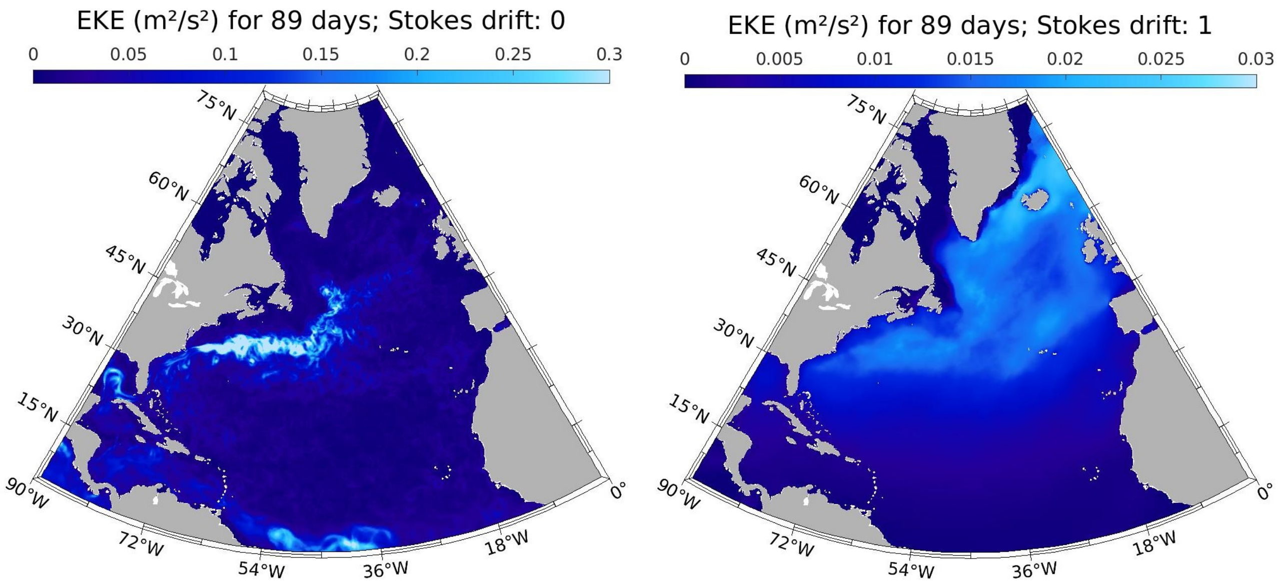


(a) The EKE for the ocean current

(b) The EKE for the Stokes drift

Figure 12: Comparison of the Eddy Kinetic Energy of (a) the ocean currents and (b) the Stoke drift over the 90 days of the Lagrangian experiments. Note the one order magnitude difference of the colorbar showing the overall weak changes of the Stoke drift compared to the ocean currents.

The dispersion error is shown in fig. 11 for each experiments, with and without Stokes drift, and at different integration times. The first thing that can be noticed, is that the error is less important for the larger time scale, which means that the linear approximation of the variance growth is a good approximation at 90-day timescale. However, as the maps show, the experiments including Stokes drift gives more errors.

While it would have been possible to think at first that the Stokes drift would bring a greater diffusivity, the results (Fig. 11) show us that this is not the case, there is little change in the diffusivity coefficient when the Stoke drift is included. To understand the spatial variations in the displacements of the particles, we first look at the amplitude of the velocity changes.

## 3.2. The Eddy Kinetic Energy (EKE)

The eddy kinetic energy is defined as half the sum of the velocity variance in each horizontal direction. This is a qualitative way of estimating the variation of the flow and hence, comparing the potential impact of ocean currents and Stokes drift on dispersion.

Figure 12 shows the energy distribution for the ocean currents only (Fig. 12a, on the left) and for the Stokes drift only (Fig. 12b, on the right). The maximum of energy is located in the Gulf Stream and in the south of the subtropical gyre for the ocean currents only. The energy of the Stokes drift is more spread spatially with higher values located near Iceland.

However, the main information is the fact that there is a factor of 10 between the EKE values of the ocean currents and of the Stokes drift. The ocean current EKE is larger than the Stokes drift EKE, which is consistent with the weak difference observed in Fig. 11 for the two experiments. Moreover, the diffusion maxima location corresponds well to the location of the maximum values of the EKE currents.

The relationship between EKE and diffusivity for all the North Atlantic ocean is investigated in Fig. 13. In the literature, there are two ways to express the link between the EKE and the

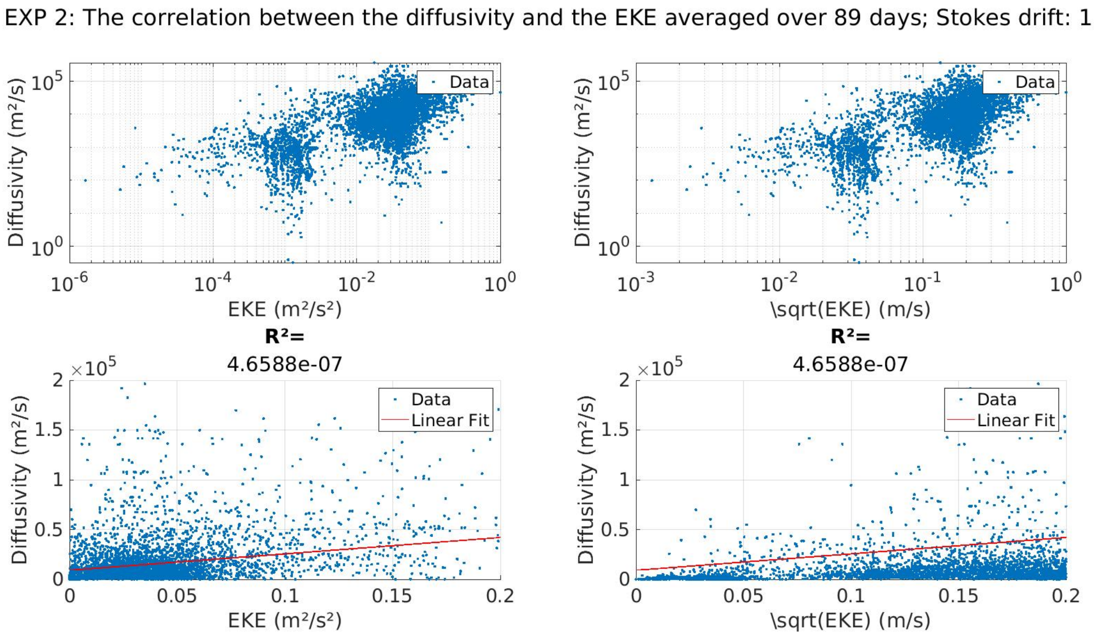


Figure 13: The relation between the diffusion and the EKE during 90 days. In the first line, the log-log representation of the diffusivity with (left) EKE and (right) squared EKE. In the second line, the diffusivity, EKE and squared EKE is plotted with linearly with the addition of the linear fit curve in red.

diffusivity (Zhurbas et al., 2014): either by $K = EKE \times T$ or by $K = \sqrt{EKE} \times L$, where $T$ and $L$ are the Lagrangian timescale and length-scale associated with mesoscale eddy turbulence, respectively. Figure 13 shows these two scalings in log and linear scale. In both cases, the low value of the $R^2$ reveals that these scalings are challenging to observe.

## 3.3. The strain stress

As demonstrated in the previous section, the strain is an important factor to show the concentration deformation. To certify that $|\Delta| \ll \sigma$, these two parameters are shown in Fig. 14 and Fig. 15. The divergence is less significant than the stretching and the shearing, and therefore negligible compared to the strain, shown in Fig. 14. Those confirm the presence of deformation. The spatial-variation of the parameters matches well with previous results of the EKE, with the main turbulence located in the Gulf Stream for the ocean currents and located on the north-eastern edge for Stokes drift. Moreover, the Stoke drift values are still ten times lower than the ocean current values.

Figure 15 compares the strain variations between one day, the $1^{st}$ of January, and an average of over 90 days for ocean currents and Stoke drift. The two results are similar for both with, however, the lower values for the averaging. The results found are not surprising for the ocean current, but for the Stokes drift, one would expect to have less small-scale feature for the mean values. Indeed, as meteorological variations are more frequent and rapid, one would not have expected to see such distinct fronts. This phenomenon might be due to the fact that the daily velocities associated with the waves are already averages of 3-hourly fields, thus smoothing the synoptic variations. Moreover, the spatial resolution of the Stokes drift being lower, a linear approximation has been made, adding physical error to this model.

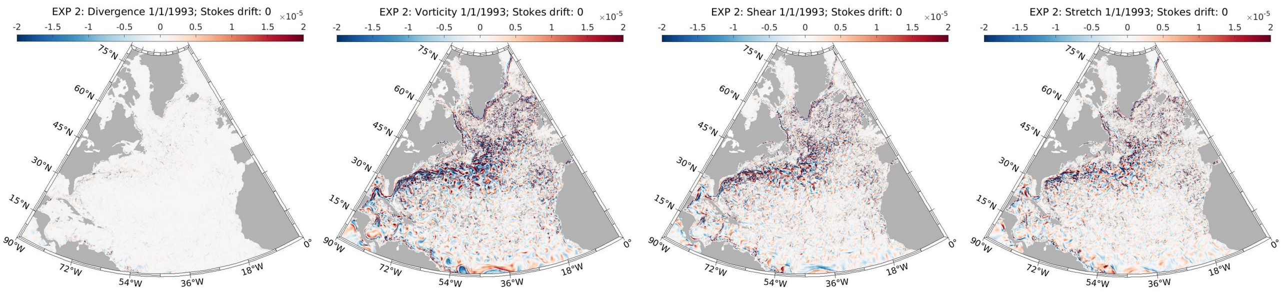


(a) Ocean current

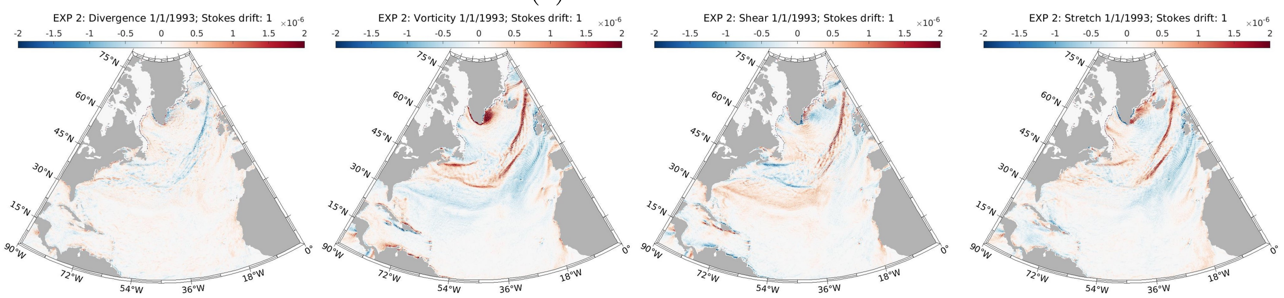


(b) Stokes drift only

Figure 14: From left to right, the divergence, the vorticity, the shearing (shear strain) and the stretching (normal strain) computed on the 1/01/1993 for (a, top row) the ocean currents and (b, bottom row) the Stokes drift.

# 4. Discussion

These first results have shown that the impact of Stokes drift on surface dispersion is not significant compared to the ocean current in the North Atlantic Ocean, however, Dobler et al. (2019) work has shown that the impact of Stokes drift deviates particles westward instead of eastward for the ocean current. By comparing these two results, we can conclude that the impact of Stokes drift depends on its nature (mean-particle displacement or particle dispersion). It might also be linked to the region of the analysis. It might be interesting in future work to look at the trend of EKE and strain in the Indian and Pacific Ocean, for comparison. Moreover, as the Stokes drift has more or less impact depending on its location, looking at other areas to get a broad overview of all the oceans, as for example in the Southern Ocean with the Antarctic Circumpolar Current.

The error on dispersion estimation is low as shown in Fig. 11, however, the higher errors are located where the Stokes drift are the strongest, like in the North of the Europe. In these locations, the linear regime assumption could be problematic. Moreover, the low values of the $R^2$ (Fig. 13) imply that there is no relation between $EKE$ or $\sqrt{EKE}$ and the diffusivity. However, the log-log scale representations can be compared to the results of Roach et al. (2018), where they study the global diffusivity from observations. They compare the theory with the drifter observations at the surface. Their Fig. 8b shows similarity with the the first row of Fig. 13.

Additionally, the maximum time considered for these experience was set to 3 months. This time can be increased avoiding the season impact on the velocities. However, increasing the time scale can increase the diffusivity error and the variance over time cannot be considered within the linear regime. To avoid this error, the simulation can run during 3 months but at different season time and analysed together.

Furthermore, vorticity has not been taken into account in this work, although some re-

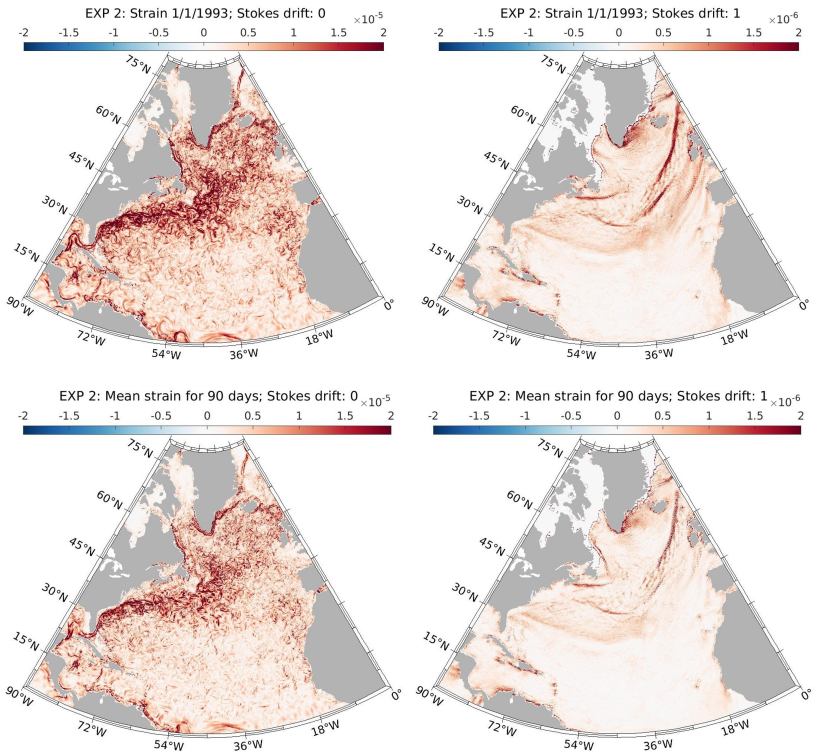


Figure 15: Strain magnitude of the ocean current (left) and of the Stokes drift (right). The first row is for the daily filed on the 1/1/1993 and the second row is averaged over the 3 months of the Lagrangian experiments.

searchers such as Vic et al. (2022) have studied the impact of the eddies on the plastic dispersion. In his paper, they explained that the cyclonic fronts are convergence zones for floating particles, which is not the case for the anticyclonic counterparts. This work was carried out by observation of drifters as well as modelling and contradicts previous papers on this subject. Here, we show that vorticity, unlike strain and divergence, is not related to tracer gradient magnitude evolution (and so change in concentration). However, the more global analogy between particle concentration zones and vorticity is also an avenue for future work, focusing not only on the North Atlantic Ocean but also on other oceans.

# 5. Conclusion

This internship allowed me to demonstrate that despite what one might have thought, adding the Stokes drift has no significant impact on the diffusivity of the floating particles. Dispersion is an easily observable phenomenon, but it is the result of many physical phenomena. This work could be continued by looking for other seasons, extending to other parts of the globe and looking more closely at the impact of eddies on particle diffusion.

In a personal conclusion, I would like to add that this internship allowed me to improve my scientific reflection. Even if these 10 weeks passed quickly, I was still able to get a fairly broad view of the parameters related to ocean surface dispersion.

# A Buoyant Tracer Gradient Dynamics *Notes from Florian Sévellec*

To study the tracer gradient dynamics, we follow the work of Okubo (1970), Weiss (1991), and Balwada et al. (2021). Hence, we start from the horizontal tracer advection equation for high Péclet number. This reads:

$$\partial_t C + \partial_x (uC) + \partial_y (vC) = 0, \tag{A.1}$$

where $C$ is the tracer concentration, $u$ and $v$ are the zonal and meridional velocities, respectively, $t$ is time, $x$ and $y$ are the longitude and latitude, respectively. Here $C$ is a conserved, buoyant tracer concentration away from sources and sinks. Since the flow is non-divergent $\partial_x u + \partial_y v + \partial_z w = 0$, we have:

$$\partial_t C + u\partial_x C + v\partial_y C = \mathcal{S}, \tag{A.2}$$

where $\mathcal{S} = -(\partial_x u + \partial_y v)C$ is the horizontal divergence of the flow acting as a source term on the horizontal advection of the tracer. Assuming that the tracer evolution is dominated by the horizontal advection rather than this source term ($|\mathcal{S}| \ll |u\partial_x C + v\partial_y C|$) we have:

$$\partial_t C + u\partial_x C + v\partial_y C = 0, \tag{A.3}$$

In the context of plastic dispersion, it is interesting to focus on the limit of a purely horizontal flow (where $\partial_z w$ is assumed to be negligible). The dynamics of tracer gradient becomes:

$$D_t \begin{pmatrix} \partial_x C \\ \partial_y C \end{pmatrix} = \mathbf{\Lambda} \begin{pmatrix} \partial_x C \\ \partial_y C \end{pmatrix}, \tag{A.4}$$

where $D_t$ ($=\partial_t + u\partial_x + v\partial_y$) is the horizontal material derivative and the $\mathbf{\Lambda}$ is flow gradient operator which reads:

$$\mathbf{\Lambda} = -\begin{pmatrix} \partial_x u & \partial_x v \\ \partial_y u & \partial_y v \end{pmatrix}. \tag{A.5}$$

We can rewrite this operator as function of properties of the flow such as:

$$\mathbf{\Lambda} = -\frac{1}{2} \begin{pmatrix} \Delta + \sigma_n & \sigma_s + \zeta \\ \sigma_s - \zeta & \Delta - \sigma_n \end{pmatrix}, \tag{A.6}$$

where $\Delta$ is the horizontal divergence, $\zeta$ is the horizontal vorticity, and $\sigma_n$ and $\sigma_s$ are the normal and shear strain (stretching and shearing), respectively. From these strain components, we can diagnose the strain magnitude ($\sigma$) as $\sigma = \sqrt{\sigma_n^2 + \sigma_s^2}$. Here $\Delta$, $\zeta$, and $\sigma$ are coordinate invariant, whereas $\sigma_n^2$ and $\sigma_s^2$ are not.

From this, we can then compute the change of the flow gradient magnitude as:

$$D_t \left[ \frac{(\partial_x C)^2 + (\partial_y C)^2}{2} \right] = (\partial_x C, \partial_y C)\, \mathbf{\Lambda} \begin{pmatrix} \partial_x C \\ \partial_y C \end{pmatrix}, \tag{A.7}$$

Since only the symmetric part will contribute to the scalar product, we have:

$$D_t \left[ \frac{(\partial_x C)^2 + (\partial_y C)^2}{2} \right] = (\partial_x C, \partial_y C)\, \mathbf{\Sigma} \begin{pmatrix} \partial_x C \\ \partial_y C \end{pmatrix}, \tag{A.8}$$

where

$$\mathbf{\Sigma} = \frac{\mathbf{\Lambda} + \mathbf{\Lambda}^\dagger}{2} = -\frac{1}{2} \begin{pmatrix} \Delta + \sigma_n & \sigma_s \\ \sigma_s & \Delta - \sigma_n \end{pmatrix}. \tag{A.9}$$

Note that this expression demonstrates that the vorticity does not contribute to magnitude changes of tracer gradient (but only to tracer gradient horizontal rotation).

From there we can decompose $\boldsymbol{\Sigma}$ by its eigenvalues and eigenvectors:

$$\boldsymbol{\Sigma} = \begin{pmatrix} p_x & s_x \\ p_y & s_y \end{pmatrix} \begin{pmatrix} \lambda_p & 0 \\ 0 & \lambda_s \end{pmatrix} \begin{pmatrix} p_x & p_y \\ s_x & s_y \end{pmatrix} \tag{A.10}$$

where $(p_x,\ p_y)$ and $(s_x,\ s_y)$ are the eigenvectors associated with the eigenvalues $\lambda_p$ and $\lambda_s$, respectively. This eigenvectors verify $p_x p_x{+}p_y p_y{=}s_x s_x{+}s_y s_y{=}1$ and, because $\boldsymbol{\Sigma}$ is symmetric, $p_x s_x{+}p_y s_y{=}s_x p_x{+}s_y p_y{=}0$.

The analytical expression of the eigenvalues is:

$$\lambda_{p/s} = -\frac{1}{2}\Delta \pm \frac{1}{2}\sigma, \tag{A.11}$$

This expression is particularly interesting since both the divergence and the strain magnitude are coordinate invariant. The sum of the two eigenvalues is the horizontal divergence (trace conservation). The eigenvectors associated with the eigenvalue $\lambda_{p/s}$ are $(\sigma_n \mp \sigma,\ \sigma_s)/\sqrt{2\sigma^2 \mp 2\sigma\sigma_n}$, this expression using $\sigma_s$ and $\sigma_n$, which are not coordinate invariant, allows for a non-trivial definition of a direction. Finally since $|\Delta|{\ll}\sigma$ (consistently with the previous assumption of weak source, $\mathcal{S}$), we find that the deformation acts, through the strain, in increasing and decreasing the gradient magnitude in two orthogonal directions. Hence the negative values measure the spreading of the concentration (damping of the tracer gradient) for which the strain is a good measure:

$$\boxed{\lambda \simeq -\frac{1}{2}\sigma,} \tag{A.12}$$

where $\lambda$ measures the rate of deformation of the tracer gradient magnitude or the spread of the concentration.

# References


Balwada, D., Xiao, Q., Smith, S., Abernathey, R., and Gray, A. R. (2021). Vertical fluxes conditioned on vorticity and strain reveal submesoscale ventilation. *Journal of Physical Oceanography*, 51:2883–2901.

Blanke, B. and Grima, N. (2005). Here follow some indications which can make easier its implementation and use! page 13.

Chenillat, F., Huck, T., Maes, C., Grima, N., and Blanke, B. (2021). Fate of floating plastic debris released along the coasts in a global ocean model. *Marine Pollution Bulletin*, 165:112116.

Dobler, D., Huck, T., Maes, C., Grima, N., Blanke, B., Martinez, E., and Ardhuin, F. (2019). Large impact of Stokes drift on the fate of surface floating debris in the South Indian Basin. *Marine Pollution Bulletin*, 148:202–209.

Lacasce, J. (2008). Statistics from lagrangian observations. *Progress In Oceanography*, 77:1–29.

Okubo, A. (1970). Horizontal dispersion of floatable particles in the vicinity of velocity singularities such as convergences. *Deep Sea Research and Oceanographic Abstracts*, 17(3):445–454.

Roach, C. J., Balwada, D., and Speer, K. (2018). Global Observations of Horizontal Mixing from Argo Float and Surface Drifter Trajectories. *Journal of Geophysical Research: Oceans*, 123(7):4560–4575.

Sévellec, F., Colin de Verdière, A., and Kolodziejczyk, N. (2022). Estimation of horizontal turbulent diffusivity from deep argo float displacements. *J. Phys. Oceanogr.*, 52:1509–1529.

Vic, C., Hascoët, S., Gula, J., Huck, T., and Maes, C. (2022). Oceanic Mesoscale Cyclones Cluster Surface Lagrangian Material. *Geophysical Research Letters*, 49(4).

Weiss, J. (1991). The dynamics of enstrophy transfer in two-dimensional hydrodynamics. *Physica D: Nonlinear Phenomena*, 48:273–294.

Zhurbas, V., Lyzhkov, D., and Kuzmina, N. (2014). Drifter-derived estimates of lateral eddy diffusivity in the World Ocean with emphasis on the Indian Ocean and problems of parameterisation. *Deep Sea Research Part I: Oceanographic Research Papers*, 83:1–11.